

Importance of Fermi surface topology for high temperature superconductivity in electron-doped iron arsenic superconductors

Chang Liu, A. D. Palczewski, Takeshi Kondo, R. M. Fernandes, E. D. Mun,
H. Hodovanets, A. N. Thaler, J. Schmalian, S. L. Bud'ko, P. C. Canfield, and A. Kaminski
Ames Laboratory and Department of Physics and Astronomy, Iowa State University, Ames, Iowa 50011, USA
(Dated: June 4, 2022)

We used angle resolved photoemission spectroscopy and thermoelectric power to study the poorly explored, highly overdoped side of the phase diagram of $\text{Ba}(\text{Fe}_{1-x}\text{Co}_x)_2\text{As}_2$ high temperature superconductor. Our data demonstrate that several Lifshitz transitions - topological changes of the Fermi surface - occur for large x . T_c starts to decrease with doping when the cylindrical, central hole pocket changes to ellipsoids centering at the Z point, and goes to zero before these ellipsoids disappear around $x = 0.2$. Changes in thermoelectric power occur at similar x -values. Beyond this doping level the central pocket changes to electron-like and superconductivity does not exist. Our observations reveal the crucial importance of the underlying Fermiology in this class of materials. A necessary condition for superconductivity is the presence of the central hole pockets rather than perfect nesting between central and corner pockets.

PACS numbers: 79.60.-i, 74.25.Jb, 74.70.Dd

The phase diagrams of the newly-discovered iron arsenic superconductors contain a number of intriguing features. For the electron-doped $A(\text{Fe}_{1-x}\text{T}_x)_2\text{As}_2$ series (122, $A = \text{Ca}, \text{Sr}, \text{Ba}$; $T = \text{Co}, \text{Ni}, \text{Pd}$, etc.), superconductivity is found in both regions with and without a long-range antiferromagnetic (AFM) order [1–7]. The superconducting (SC) region extends to different doping levels for different dopants, but scales very well if the horizontal axis of the phase diagram was chosen to be the number of extra electrons [6, 7]. It is therefore likely that changes in the underlying electronic structure due to electron doping are linked closely to their SC behavior. On the underdoped side, a recent angle-resolved photoemission spectroscopy (ARPES) study on $\text{Ba}(\text{Fe}_{1-x}\text{Co}_x)_2\text{As}_2$ [8] revealed that superconductivity emerges at a doping level (x_{on}) where a topological change of the Fermi surface (Lifshitz transition [9] at doping x_1) reduces the magnetically reconstructed Fermi surface to its paramagnetic appearance, i.e. $x_1 \approx x_{\text{on}}$. This transition exhibits itself as a rapid change of Hall coefficient and thermoelectric power (TEP) in transport measurements [10]. An immediate question is whether a similar change of Fermiology causes the collapse of the SC dome on the heavily overdoped regime. It is inevitable that the hole pockets surrounding the central axis of the Brillouin zone (Γ - Z) will shrink in size and vanish at some higher doping x_2 . The question is whether this Lifshitz transition correlates with the offset of superconductivity on the overdoped side of the phase diagram (x_{off}). Based on a solution of the two-band BCS gap equations, assuming only interband coupling, Fernandes and Schmalian [12] showed that the disappearance of superconductivity is directly linked to the vanishing of the central hole pocket(s), i.e. $x_2 \approx x_{\text{off}}$. Experimentally, the Hall coefficient vs. doping on $\text{Ba}(\text{Fe}_{1-x}\text{Co}_x)_2\text{As}_2$ [4] experiences a slight change of slope around x_{off} , hinting at a possible Lifshitz transition

close to the high doping offset of superconductivity.

In this Letter we study this issue in detail using ARPES and TEP measurements. We performed a complete survey of the electronic structure on the overdoped part of the phase diagram of this material. This survey reveals that topological changes of the Fermi surface link directly to superconductivity in electron-doped pnictides. In the overdoped side, superconducting transition temperature T_c starts to be suppressed around the doping level ($x_{2\Gamma}$) where the cylindrical hole pocket surrounding the zone center (Γ - Z) changes to ellipsoids centering at Z . T_c is driven to zero before the disappearance of

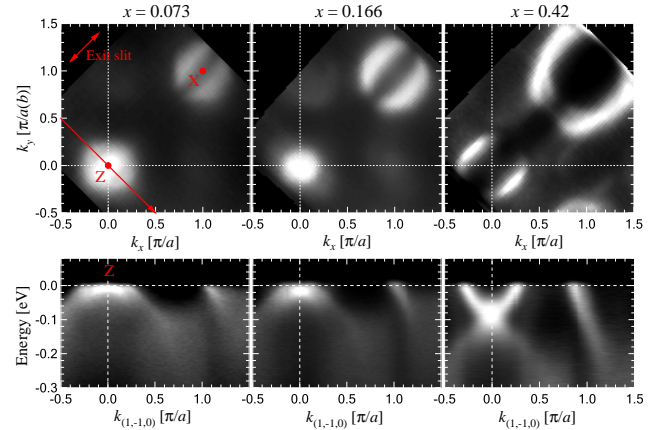


FIG. 1: (Color online) Fermi maps and band dispersion around the upper zone edge Z of $\text{Ba}(\text{Fe}_{1-x}\text{Co}_x)_2\text{As}_2$ for $x = 0.073$ (optimal doping), $x = 0.166$ (edge of SC dome) and $x = 0.42$. Upper Row: Fermi mappings for the three doping levels, taken with incident photon energy $h\nu = 35$ eV at temperature $T = 20$ K. Red arrows show the exit slit direction of the hemispheric analyzer and the cutting direction of the band dispersion maps (Lower Row). The same direction is also used in Fig. 2.

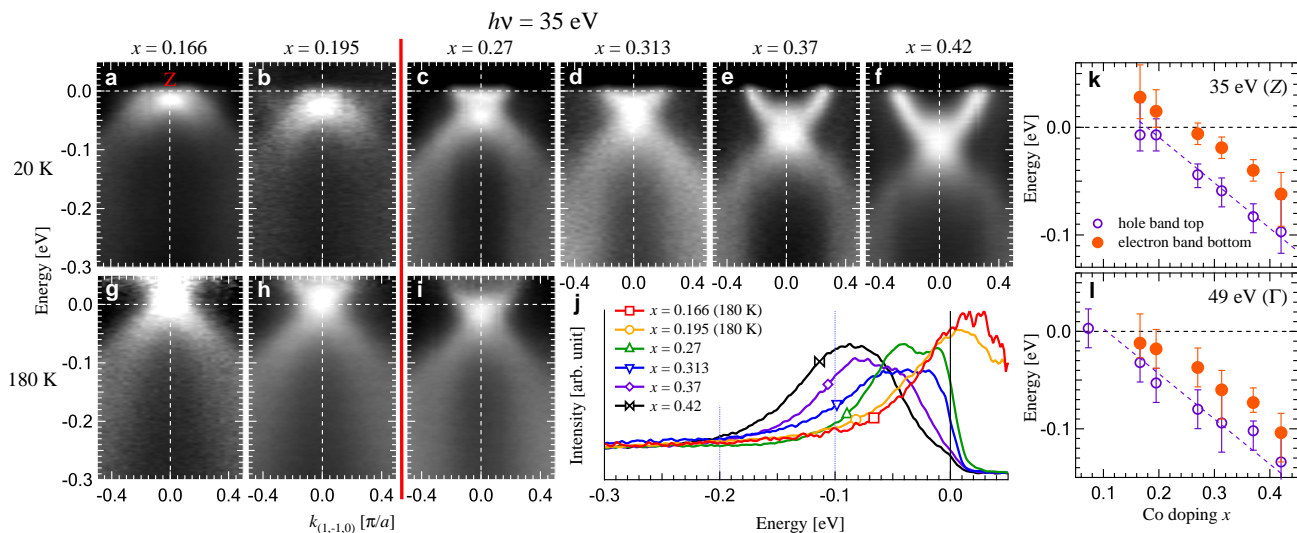


FIG. 2: (Color online) Band location analysis for the Lifshitz transitions. (a)-(i): Band dispersion maps along the direction shown in Fig. 1 for six different doping levels (top of each column) at low and high temperatures (left of each row). All data is taken with 35 eV photons. The high temperature data is divided by the resolution convoluted Fermi-Dirac function for better pinpointing the band positions above the Fermi level. The red vertical line indicates that a Lifshitz transition happens between $x = 0.195$ and $x = 0.27$ at Z . (j) Energy distribution curves (EDCs) at Z for the doping levels in panels (a)-(i). Measurement temperature is $T = 20$ K unless specifically mentioned in the graph. (k),(l): Evolution of binding energy for the top of the hole band and the bottom of the electron band with respect to cobalt doping. Data is extracted from ARPES intensity maps taken with (k) 35 eV and (l) 49 eV photons, corresponding to k_z values of Z and Γ points, respectively. Data points in (k) are extracted from the EDCs at (j) by fitting with two Lorentzian functions (times the Fermi function for low temperature data). Raw data for extracting panel (l) is not shown.

Z -ellipsoids and the change in TEP at $x_{2Z} \sim 0.2$. In short, we find that $x_{2\Gamma} < x_{\text{off}} < x_{2Z}$. Our data demonstrated that superconductivity in the pnictides is very robust with respect to doping; the whole Γ Fermi sheet has to be almost completely eliminated in order to drive T_c to zero. A necessary condition for superconductivity then is the existence of the central hole pockets rather than a perfect nesting between the Γ and X pockets [11]. The dominant contribution to the pairing interaction is believed to come from inter-band coupling [12].

Single crystals of $\text{Ba}(\text{Fe}_{1-x}\text{Co}_x)_2\text{As}_2$ were grown out of a self-flux using conventional high-temperature solution growth techniques [1]. The doping level x was determined using wavelength dispersive X-ray spectroscopy in a JEOL JXA-8200 electron microprobe [1]. Long range antiferromagnetism was observed below a transition temperature $T_N(x)$ up to $x \sim 0.06$. Superconductivity appears around $x_{\text{on}} = 0.038$ and vanishes between $0.135 < x_{\text{off}} \leq 0.166$ (see Fig. 4) [7]. The ARPES measurements were performed at beamline 10.0.1 of the Advanced Light Source (ALS), Berkeley, California using a Scienta R4000 electron analyzer. Vacuum conditions were better than 3×10^{-11} torr. The energy resolution was set at ~ 25 meV. All samples were cleaved *in situ* yielding mirror-like, fresh a - b surfaces. High symmetry points were defined the same way as in Ref. [8]. TEP measurements were made as described in Ref. [10].

Fig. 1 shows the ARPES Fermi maps and corresponding band dispersion data for three different doping levels of $\text{Ba}(\text{Fe}_{1-x}\text{Co}_x)_2\text{As}_2$ [13]. The incident photon energy is $h\nu = 35$ eV, corresponding to $k_z \simeq 2\pi/c$, the upper edge of the first Brillouin zone (Z) [14]. From data in Fig. 1 it is clear that, as electron doping initially increases, the Fermi contours around Z shrink in size. At $x = 0.166$, the edge of the SC dome, the Z -pocket shrinks to almost a single point, meaning a complete vanishing of the hole pocket. This observation is consistent with the data in Refs. [8, 15, 16]. As x increases, the Z pocket expands again, yielding a diamond shape at $x = 0.42$. Band dispersion clearly reveals that this “diamond” is electron-like. Such an electron pocket is not predicted by band structure calculations [4]. The X pocket, on the other hand, keeps expanding from $x = 0.073$ to $x = 0.42$, and it remains electron-like. The central message of this figure is that the Z -pocket undergoes a drastic topological change from hole-like to electron-like at roughly the doping level where superconductivity vanishes. Based on this observation we perform two independent data analysis procedures with finer doping steps to further pinpoint the doping level at which the Lifshitz transition takes place.

First, to obtain a more accurate value for x_2 , we extract the energies for the hole band top and the electron band bottom at the zone center, and examine them as

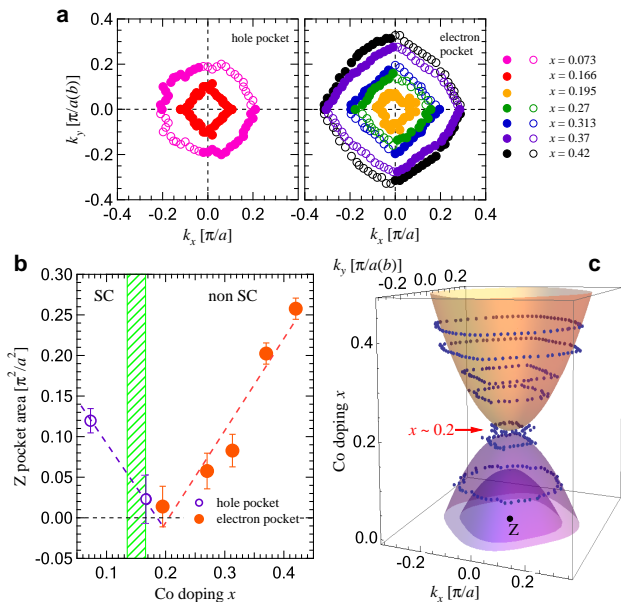


FIG. 3: (Color online) Pocket size analysis for the Lifshitz transition at upper zone boundary Z . (a) Z pocket extraction for seven doping levels, done by fitting the momentum distribution curves (MDCs) at the chemical potential with several Lorentzian functions. Positions of hollow circles are symmetrized from experimental data points (solid circles), proposing the band positions where ARPES intensity is suppressed by the transition matrix element. (b) Evolution of Z pocket area with cobalt doping. Green shaded area indicates the boundary of the SC dome. (c) Visualization of the Lifshitz transition. Data in (a) is plotted against the cobalt doping x as a third dimension. Shaded areas are approximate size and shape of the pockets. Panels (b) and (c) show a Lifshitz transition at $x_{2Z} \sim 0.2$.

a function of cobalt doping. As shown in Fig. 2, we plot the band dispersion maps along the same direction as in Fig. 1 for six different doping levels ranging from $x = 0.166$ to $x = 0.42$, and use the energy distribution curves (EDCs) in Fig. 2(j) [17] to see that both the hole band and the electron band shift to higher binding energies as x increases. The shape of these bands remain the same during the process. There is a small gap (~ 25 meV) between these two bands. At $0.195 < x < 0.27$ the bottom of the electron band moves above the Fermi level, as revealed in Fig. 2(k) where two Lorentzians are fitted to the data from Fig. 2(j). At a slightly lower doping level the top of the hole pocket also moves above E_F . Figs. 2(a)-(k) illustrate that, at the Z point of the Brillouin zone, the Lifshitz transition takes place between $0.195 < x_{2Z} < 0.27$, higher than $x_{\text{off}} \sim 0.15$.

The intrinsic three dimensionality of the electronic structure [18, 19] results in different x_2 values for different k_z . In Fig. 2(l) we investigate this effect by performing the same analysis to the data taken with 49 eV photons (raw data not shown). This incident photon energy cor-

responds to $k_z \simeq 0$, the central point of the Brillouin zone (Γ). We see that indeed the Lifshitz transition shifts to a lower doping, i.e. $x_{2\Gamma} \sim 0.11$. We note that this is the doping level where T_c starts to decrease in the phase diagram. This observation also supports the theoretical prediction that three dimensionality of the Fermi surface leads to a more gradual decrease of T_c in the overdoped side [12].

In Fig. 3 we perform a pocket size analysis at Z to further pinpoint x_2 . This second procedure is independent from the above energy extraction method. To do this we first find the Z pocket location for seven doping levels (ranging from $x = 0.073$ to $x = 0.42$) by fitting the momentum distribution curves (MDCs) at the chemical potential with several Lorentzian functions. From Fig. 3(a) we see a clear evolution of the Z pocket size with doping. As x increases, the hole pocket shrinks in size up to $x = 0.195$. Above this doping an electron pocket appears and increases in size up to the highest doping measured. As seen in Fig. 3(b), both the hole and electron pocket size evolves in a linear fashion, a signature of the validity of the rigid band shifting scenario [20], and of the pockets being paraboloids in shape. The crossover takes place around $x = 0.2$. This Lifshitz transition is best visualized in Fig. 3(c) where data in Fig. 3(a) is plotted against the cobalt doping x as a third dimension. This figure reveals that, as cobalt concentration increases, the Fermi sea level rises and the Z hole bands gradually drop below it. At $x \sim 0.2$ the total occupation of the outer hole band marks the Lifshitz transition. Beyond this point the Z pocket changes to electron-like, and superconductivity vanishes.

Fig. 4 summarizes our systematic ARPES survey on the Fermi surface topology of $\text{Ba}(\text{Fe}_{1-x}\text{Co}_x)_2\text{As}_2$ for $0 \leq x \leq 0.42$ and compares it with TEP data over the same doping range. The most important finding of this study is that the low- and high-doping onset of the SC region link closely to topological changes of the Fermi surface. The first Lifshitz transition at the low doping onset of superconductivity is described in detail in Ref. [8, 10]. The second and third Lifshitz transitions occur for $0.11 \lesssim x \lesssim 0.2$ and correspond to the high doping onset of superconductivity. $x_{2\Gamma} \simeq 0.11$ corresponds to the doping level where the shape of the quasi-cylindrical outer Γ contour changes to an ellipsoid centering at Z . Also at $x \simeq 0.11$ the superconducting T_c starts to suppress. As doping is increased, this Z ellipsoid shrinks in size until it disappears altogether at $x_{2Z} \simeq 0.2$. On the other hand, superconductivity vanishes at $x_{\text{off}} \simeq 0.15$. At $x > 0.2$, the region of the highest doping, the central pocket changes to electron-like, and superconductivity does not exist. Our TEP data, plotted as $S(x)|_{T=\text{const}}$ for several temperatures in Fig. 4(b), show clear step-like or change-of-slope anomalies at Co-concentrations that are in an excellent agreement with those at which the Lifshitz transitions were detected by ARPES [Fig. 4(a)].

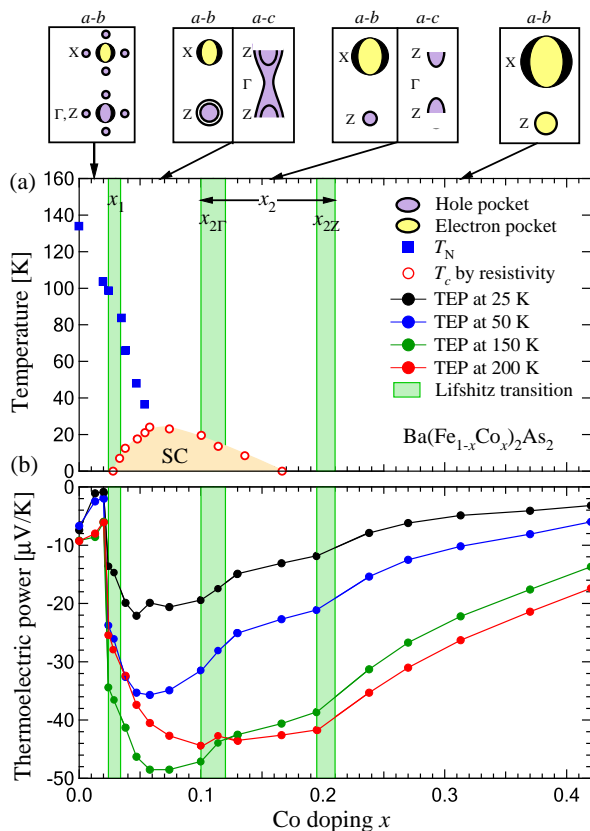


FIG. 4: (Color online) (a) location of the known Lifshitz transitions in the phase diagram. T_N and T_c data is taken from Refs. [1] and [8]. Top insets show schematic Fermi surface topology in the a - b and a - c plane for each region in the phase diagram. (b) Thermoelectric power vs. doping for four different temperatures.

These results, taken together, confirm extreme sensitivity of TEP to the changes in FS topology [21].

Importantly, the above conclusion most likely also applies to other electron doped 122 systems. We are specially interested in $A(\text{Fe}_{1-x}\text{Ni}_x)_2\text{As}_2$ where each nickel atom gives two extra electrons per Fe site compared to one in the cobalt doped system [7]. There, similar to the cobalt doped system, the Hall coefficient and thermoelectric power anomaly occurs right at the onset of superconductivity [8, 22]. Based on a similar ARPES survey [23] we indeed find Lifshitz transitions at close vicinity to the boundaries of superconductivity, the only difference being that the corresponding doping levels are roughly one half as those of the cobalt system. As the phase diagram changes to T vs. e , the extra electron count, these two systems match perfectly.

Our findings have important implications on the nature of superconductivity of the pnictides. First, our observation reveals the crucial importance of the underlying Fermi surface topology: a necessary condition for the emergence of superconductivity is the existence of

the non-reconstructed central hole pockets rather than a perfect nesting condition between the central and corner pockets. Superconductivity is not supported only when either one set of these pockets (central or corner) vanishes, changes its carrier nature or shows considerable reconstruction. Second, our results imply that the suppression of superconductivity on the underdoped side is related to the competition between the AFM and SC phases [7], whereas on the overdoped side the disappearance of the central hole pocket plays a more important role than the decrease of the pairing interaction magnitude [12]. Electron doped 122 systems are, therefore, clear examples of high temperature superconductors whose superconducting behavior is controlled primarily by the underlying Fermiology.

We thank Sung-Kwan Mo and Makoto Hashimoto for their grateful instrumental support at the ALS. Ames Laboratory was supported by the Department of Energy - Basic Energy Sciences under Contract No. DE-AC02-07CH11358. ALS is operated by the US DOE under Contract No. DE-AC03-76SF00098.

- [1] N. Ni *et al.*, Phys. Rev. B **78**, 214515 (2008).
- [2] J.-H. Chu, J. G. Analytis, C. Kucharczyk, and I. R. Fisher, Phys. Rev. B **79**, 014506 (2009).
- [3] F. L. Ning *et al.*, J. Phys. Soc. Jpn. **78**, 013711 (2009).
- [4] L. Fang *et al.*, Phys. Rev. B **80**, 140508(R) (2009).
- [5] S. Nandi *et al.*, Phys. Rev. Lett. **104**, 057006 (2010).
- [6] P. C. Canfield *et al.*, Phys. Rev. B **80**, 060501(R) (2009).
- [7] P. C. Canfield and S. L. Bud'ko, Annu. Rev. Condens. Matter Phys. **1**:11.1-11.24 (2010).
- [8] C. Liu *et al.*, Nature Physics **6**, 419 (2010).
- [9] I. M. Lifshitz, Sov. Phys. JETP **11**, 1130 (1960).
- [10] E. D. Mun, S. L. Bud'ko, N. Ni, and P. C. Canfield, Phys. Rev. B **80**, 054517 (2009).
- [11] K. Terashima *et al.*, Proc. Natl. Acad. Sci. USA **106**, 7330 (2009).
- [12] R. M. Fernandes and J. Schmalian, Phys. Rev. B **82**, 014521 (2010).
- [13] Direction of the band dispersion maps is perpendicular to the exit-slit because the ARPES intensity of the Z electron pocket along the exit-slit direction is suppressed by the transition matrix element.
- [14] T. Kondo *et al.*, Phys. Rev. B **81**, 060507(R) (2010).
- [15] Y. Sekiba *et al.*, New J. Phys. **11**, 025020 (2009).
- [16] V. Brouet *et al.*, Phys. Rev. B **80**, 165115 (2009).
- [17] In Fig. 2(j) high temperature data divided by the Fermi function is used for $x = 0.166$ and $x = 0.195$ in order to better locate the band positions above E_F .
- [18] C. Liu *et al.*, Phys. Rev. Lett. **102**, 167004 (2009).
- [19] P. Vilmercati *et al.*, Phys. Rev. B **79**, 220503(R) (2009).
- [20] M. Neupane *et al.*, arXiv:1005.2966 (2010).
- [21] Y. M. Blanter, M. I. Kaganov, A. V. Pantsulaya, and A. A. Varlamov, Phys. Reports **245**, 159 (1994).
- [22] N. P. Butch *et al.*, Phys. Rev. B **81**, 024518 (2010).
- [23] A. D. Palczewski *et al.*, in preparation.